Acta Crystallographica Section D
Biological Crystallography
ISSN 0907-4449

The structure of human mitochondrial branched-chain aminotransferase

Neela Yennawar,[a]* Jennifer Dunbar,[a] Myra Conway,[b] Susan Hutson[b] and Gregory Farber[a]

[a]Department of Biochemistry and Molecular Biology, Penn State University, University Park, PA 16802, USA, and [b]Department of Biochemistry, Wake Forest University School of Medicine, Winston-Salem, North Carolina 27157, USA

Correspondence e-mail: nhy1@psu.edu

Received 4 September 2000
Accepted 29 January 2001

PDB References: human BCATm: orthorhombic, 1ekf; trigonal, 1ekv; monoclinic, 1ekp.

X-ray crystal structures of three forms of human mitochondrial branched-chain aminotransferase (BCAT) were solved by molecular-replacement methods, using *Escherichia coli* BCAT as the search model. The enzyme is a homodimer and the polypeptide chain of each monomer has two domains. The small domain is composed of residues 1–175 and the large domain is composed of residues 176–365. The active site is close to the dimer interface. The 4′-aldehyde of the PLP cofactor is covalently linked to the ε-amino group of the active-site lysine, Lys202, *via* a Schiff-base linkage in two of the structures. In the third structure, the enzyme is irreversibly inactivated by Tris. The overall fold of the dimer in human mitochondrial BCAT is similar to the structure of two bacterial enzymes, *E. coli* BCAT and D-amino acid aminotransferase (D-AAT). The residues lining the putative substrate-binding pocket of human BCAT and D-AAT are completely rearranged to allow catalysis with substrates of opposite stereochemistry. In the case of human mitochondrial branched-chain aminotransferase, a hydrogen-bond interaction between the guanidinium group of Arg143 in the first monomer with the side-chain hydroxyl of Tyr70 in the second monomer is important in the formation of the substrate-binding pocket.

1. Introduction

Branched-chain aminotransferase (BCAT; E.C. 2.6.1.42) catalyzes the transamination of the branched-chain amino acids leucine, isoleucine and valine to their respective α-keto acids, α-ketoisocaproate, α-keto-β-methylvalerate and α-ketoisovalerate. The enzyme requires pyridoxal 5′-phosphate (PLP) as a cofactor to catalyze this reaction. BCAT proteins have been purified from a number of mammals and bacteria; the cDNA sequences of BCATs from a large number of species including rat, sheep and humans have become available (Ichihara, 1985; Wallin *et al.*, 1990; Hall *et al.*, 1993; Hutson *et al.*, 1995; Schuldiner *et al.*, 1996; Bledsoe *et al.*, 1997; Faure *et al.*, 1999). Hutson and coworkers have established that mammals contain both a mitochondrial and a cytosolic form of the enzyme, while bacteria contain only one form of the enzyme (Hutson *et al.*, 1988, 1995; Davoodi *et al.*, 1998). The mitochondrial branched-chain aminotransferase (BCATm) plays a significant role in skeletal muscle glutamine and alanine synthesis and in interorgan nitrogen metabolism (reviewed in Harper, 1989). Recently, the BCAT isoenzymes have received renewed interest because the anticonvulsant drug gabapentin is a competitive inhibitor of the cytosolic isoenzyme, which is localized almost exclusively in the central

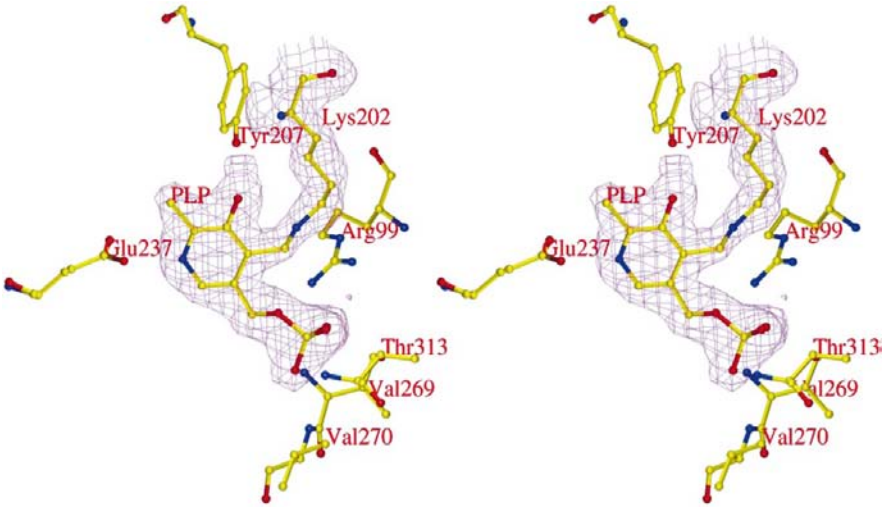

Figure 1
Active-site diagram showing Lys202 covalently linked to the PLP and a $2F_o - F_c$ electron-density map contoured at the 1.3σ level after refinement. Key residues interacting with the PLP are shown.

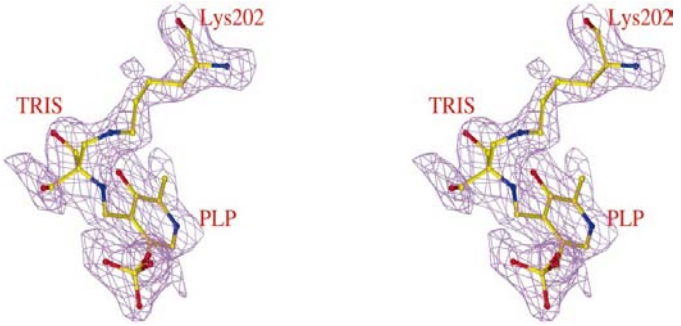

Figure 2
Active-site density of BCAT inhibited by Tris. The map was calculated from a structure that does not contain Tris. This is the first example in the Protein Data Bank where a buffer has formed a covalent intermediate with an enzyme active site.

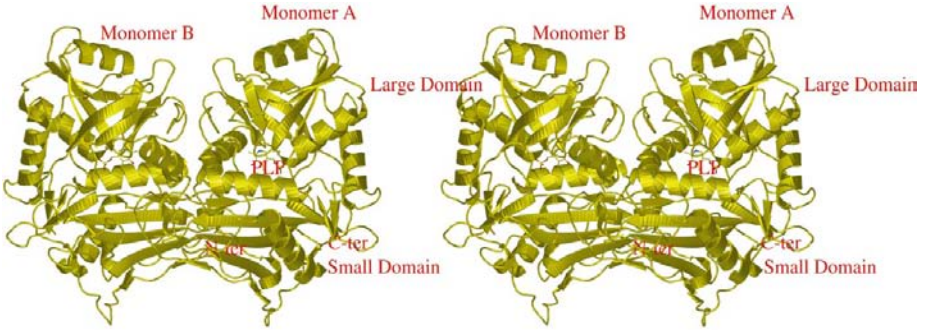

Figure 3
Ribbon diagram of human BCATm generated using the program *O* (Jones & Kjeldgaard, 1997).

nervous system (Hutson *et al.*, 1998). The mitochondrial isoenzyme, BCATm, is not a target of the drug. Since neurotransmitter pools of glutamate and γ-aminobutyric acid, which is synthesized from glutamate, may be derived from metabolic pools formed by BCAT (Hutson *et al.*, 1998), it is thought that inhibition of the cytosolic BCAT by gabapentin may be important in the mechanism of action of this drug (Welty *et al.*, 1995; Hutson *et al.*, 1998).

Aspartate aminotransferases from several species have been extensively studied using biochemical and X-ray crystallographic methods (Ichihara, 1985; McPhalen *et al.*, 1992; Malashkevich *et al.*, 1993, 1995; Jager *et al.*, 1994; Okamoto *et al.*, 1994; Miyahara *et al.*, 1994). The structure of BCAT from *E. coli* (Okada *et al.*, 1997), the recent structure of 4-amino-4-deoxychorismate lyase from *E. coli* (Nakai *et al.*, 2000) and the structure of D-amino acid aminotransferase (D-AAT; Sugio *et al.*, 1995) have provided insight into the mechanism of both of these enzymes. Although their substrates have different stereochemistry, these proteins are classified as fold-type IV PLP-dependent enzymes (Grishin *et al.*, 1995). A unique feature of this class of PLP-dependent enzymes, in contrast to other PLP enzymes and the fold-type II aspartate aminotransferases, is that the C-4′ hydrogen transfer of the coenzyme–substrate imine intermediate occurs on the *Re* face instead of the *Si* face of the enzyme (Yoshimura *et al.*, 1993).

Both the mitochondrial and cytosolic human BCATs have been overexpressed and characterized by Davoodi *et al.* (1998). The present paper describes the crystallization and three-dimensional structure of human mitochondral BCAT (BCATm) in three crystal forms. The monoclinic and orthorhombic forms have the PLP covalently bound in the active site. The trigonal form has Tris covalently linked to the PLP at one end and to the active-site lysine at the other. Comparison of the structures with that of the *E. coli* BCAT reveals key similarities in the active site although they share only 28.9% sequence identity. Further comparison with D-AAT provides a deeper insight into the method by which this class of PLP-containing enzymes catalyses similar reactions with substrates of opposite stereospecificity (Grishin *et al.*, 1995).

2. Materials and methods

The expression of human mitochondrial BCAT in *E. coli*, removal of the histidine tag by thrombin cleavage and purification of the expressed enzyme have been reported by Davoodi *et al.* (1998). The recombinant protein contains four additional residues at the N-terminus (GSHM) (Davoodi *et al.*, 1998). These residues were not well defined in the electron-density map and are not included in the BCATm structure or the numbered amino-acid sequence alignment shown in Fig. 3.

Crystals of human recombinant BCATm were obtained using the vapour-diffusion method with hanging drops at room temperature. The drops consisted of 5 µl of protein solution (pale yellow) and 5 µl reservoir. The drop was equilibrated against 1 ml of the reservoir. The protein solution contained 2.5 mg ml^{-1} BCAT in a solution of 50 m*M* HEPES pH 7.0, 20 m*M* DTT and 50 m*M* EDTA. Crystals, some yellow in color and some clear, grew readily in about 1–2 weeks in several conditions using the Hampton crystallization reagent kit. Yellow crystals grew in grids set up with 22–30% PEG 1500, 100 m*M* HEPES pH 6.9–7.2 and 20 m*M* DTT. The yellow color is characteristic of an active site in which the PLP is covalently linked to the catalytic lysine. Yellow crystals also grew with 1.6 *M* sodium or potassium phosphate, 20 m*M* DTT and 0.1 *M* HEPES pH 7.0 in the reservoir. These crystals were of monoclinic form and exhibited $P2_1$ space-group symmetry. There was a dimer in the asymmetric unit.

When HEPES was replaced by Tris in order to explore the effect of higher pH on the yellow crystals grown from the PEG 1500 condition, the crystals that grew were colorless. The clear color indicated that the enzyme had either lost the cofactor or that some reaction involving PLP had occurred. Colorless crystals suitable for diffraction experiments grew when the reservoir consisted of 2.4 *M* ammonium sulfate and 20 m*M* DTT in 100 m*M* Tris pH 8.2. Tris was the key molecule in common with the PEG condition mentioned above that also resulted in clear crystals. When characterized, these crystals were found to belong to the trigonal space group $P3_2$, with a dimer in the asymmetric unit.

Room-temperature data were collected from the yellow monoclinic crystals using a Rigaku RU-200 rotating-anode X-ray generator (operated at 100 mA and 50 kV) and an R-AXIS II area detector. Indexing, integration, reduction and scaling of the X-ray data were carried out using the program *DENZO* (Otwinowski & Minor, 1996). Crystal data parameters are listed in Table 1. These crystals diffracted to 2.5 Å.

Low-temperature data (223 K) were collected from clear crystals that had been flash-frozen. The clear crystals were soaked in a cryobuffer containing 10% each of glycerol and glucose in the crystallization condition for about 12 h before flash-freezing. The X-ray source used was a Rigaku RU-200 and data were collected using an R-AXIS IV area detector. Indexing, integration, reduction and scaling of the X-ray data were carried out using the program *DENZO* (Otwinowski & Minor, 1996) as before. The resolution of the data, 2.3 Å, was slightly better than with the PLP crystals. Since the starting model for molecular replacement, *E. coli* BCAT, had low sequence homology to the human enzyme, both this and the earlier data sets were just sufficient to solve the initial phase problem but were not good enough to complete the refinement.

In an attempt to obtain better crystals, more grids were set up with the previously described PEG condition in an identical fashion, with a freshly purified batch of protein. Yellow crystals grew as before but when characterized turned out to belong to a different space group, orthorhombic $P2_12_12_1$. These were flash-frozen with a soaking solution of the crystallization condition having 10% glycerol added to it so as to obtain a glassy freeze. Diffraction data to 1.95 Å resolution were collected at the synchrotron source at the Advanced Light Source on beamline 5.0.2 with a 2 × 2 array CCD detector, using 1.071 Å wavelength radiation monochromated with a double-crystal Si(111). *DENZO* and *SCALEPACK* were used to reduce the data.

Table 1
Crystallographic data-collection and refinement statistics for human BCATm in the three forms.

	Orthorhombic	Monoclinic	Trigonal
Space group	$P2_12_12_1$	$P2_1$	$P3_2$
Unit-cell parameters			
a (Å)	69.4	59.6	83.7
b (Å)	105.0	111.6	83.7
c (Å)	107.0	59.9	104.8
α (°)	90.0	90.0	90.0
β (°)	90.0	95.89	90.0
γ (°)	90.0	90.0	120.0
No. of unique reflections	57217	27009	37970
No. of reflections refined	48329	21221	31159
Resolution (Å)	1.95	2.5	2.3
Completeness (%)	83.8	78.6	82.1
Crystallographic *R*	0.22	0.16	0.21
Free *R* factor	0.26	0.22	0.27
No. of protein atoms	5812	5812	5812
No. of Tris atoms	0	0	14
No. of PLP atoms	30	30	30
No. of waters	273	197	212
Ramachandran plot			
Core (%)	87.6	88.3	87.5
Allowed region (%)	12.2	11.6	12.1
Disallowed region (%)	0.2	0.2	0.5
Mean *B* factors			
All atoms	33.9	26.6	18.7
Main chain	32.7	25.4	17.9
Side chain	35.0	27.8	19.5
PLP	27.3	19.8	19.2
Waters	35.5	28.8	19.5
R.m.s.d. from ideal			
Bonds (Å)	0.009	0.008	0.012
Angles (°)	1.584	1.332	1.708

2.1. Structure determination

All the crystal forms have a dimer in the asymmetric unit. Molecular-replacement attempts failed when a monomer of *E. coli* BCAT or D-AAT or a dimer of D-AAT were used as search models. A BCAT dimer search model was constructed using a crystallographically related monomer of *E. coli* BCAT (operator $-x, \frac{1}{2}+y, -z$; translation $-1, 0, -1$). The poly-Ala backbone atoms of the dimer, when used as the input model in the program *AMoRe* (Navaza, 1994) with the monoclinic data, yielded a possible solution. This solution had a high *R* factor (51.2%) and a poor correlation coefficient (18.4), but it was separated from other solutions. It was a challenging task to refine this model, since the crystallographic and free *R* factors after rigid-body and slow-cooling refinement in *X-PLOR* (Brünger, 1992) were 52.5 and 53.2% at 3.2 Å and the maps looked very noisy in *O* (Jones & Kjeldgaard, 1997; Kleywegt & Jones, 1997). The phases needed to be improved considerably in order to start building the model. The phase improvement

began with several cycles of non-crystallographic symmetry matrix refinement along with rigid-body refinement using the program *RESTRAIN* (Howlin *et al.*, 1993) from the *CCP*4 suite (Collaborative Computational Project, Number 4, 1994). The resolution in *RESTRAIN* was gradually increased from 4.0 to 3.5 to 3.0 Å in each macrocycle. Further, the rigid-body refinement was progressively changed from dimer to monomer to subunits to helices and sheets. Next the electron density was modified by utilizing the non-crystallographic symmetry for density averaging of the dimer and solvent flattening using the program *DM* (Cowtan & Main, 1996). After dozens of iterations of model building using *O* (Jones & Kjeldgaard, 1997) and refinement using *X-PLOR* (Brünger, 1992) followed by density modification using *DM*, the free *R* factor and crystallographic *R* factor gradually decreased to 38 and 35%, respectively. At this point, there were still about 40 residues at the N-terminus missing from the model. Density for these was not seen with the 2.5 Å data we obtained from the monoclinic structure. In order to model this, the structure of the trigonal form (using low-temperature data to 2.3 Å) was solved by molecular-replacement methods using the backbone atoms of the *E. coli* BCAT poly-Ala dimer in the program *AMoRe*. As before, the refinement of this structure did not progress beyond a free *R* factor and crystallographic *R* factor of around 38 and 35%, respectively. The density for the missing residues could still not be traced. There was a need for higher resolution data. This was collected using a synchrotron with crystals grown in the orthorhombic form.

Molecular replacement with the *E. coli* BCAT poly-Ala dimer model which had solved the phase problem with the monoclinic and the trigonal data did not give any solution with the orthorhombic data. The partially refined trigonal form BCAT structure, with many of the side chains modelled, served as a good search model in molecular replacement when either a monomer or a dimer was used. The correlation coefficient was as high as 35.8 with the monomer alone. The molecular-replacement method unambiguously assigned the space group to be $P2_12_12_1$ and not any of the other possibilities in the *P*222 family. Rigid-body refinement using *AMoRe* was alternated by torsion-angle slow-cooling refinement in *CNS* (Brunger *et al.*, 1998) in three increasing resolution steps, 4.0, 3.5 and 3.0 Å. The entire model was scrutinized by composite omit σ-map calculation in *CNS*. The NCS restraints on the dimer were then relaxed and the 40 or so residues at the N-terminus and the remaining side chains could be gradually modelled in subsequent difference Fourier maps using the program *O*. A $2F_o - F_c$ map of the active site unambiguously showed a covalently bound pyridoxal 5′-phosphate (Fig. 1). Water molecules were picked up on the basis of the peak heights and distance criteria from a $2F_o - F_c$ map using the water-picking routine in *CNS*. Further model-building and refinement cycles resulted in an $R_{\rm free}$ of 26.0% and an $R_{\rm cryst}$ of 22.0% using 48 329 reflections to 1.95 Å with a 2σ cutoff on *F* (Table 1). The final model comprises 2 × 365 residues, two PLPs and 273 water molecules. The success of the approach is remarkable, since the comparable secondary-structure elements of the main-chain atoms of *E. coli* BCAT dimer with the human BCATm comprise only 20.5% of the atoms in the asymmetric unit.

```
ecolibcat,1-11     ~~~~~~~~~~ ~~~~~~~~~~ ~~~~~~~~~~ ~~~~~~~~~T TKKADYIWFN
  dalanine,1-6     ~~~~~~~~~~ ~~~~~~~~~~ ~~~~~~~~~~ ~~~~~~~~~~ ~~~~GYTLWN
humanbcatm,1-50    ASSSFKAADL QLEMTQKPHK KPGPGEPLVF GKTFTDHMLM VEWNDKGWGQ
                                                                        .

 ecolibcat,12-60   GEMVRWEDAK VHVMSHALHY GTSVFEGIRC YDSHKGPVLV FRHREHMQRL
  dalanine,7-51    DQIVKDEEVK IDKEDRGYQF GDGVYEVVKV YNGE.....M FTVNEHIDRL
humanbcatm,51-100  PRIQPFQNLT LHPASSSLHY SLQLFEGMKA FKGKDQQVRL FRPWLNMDRM
                     .  ..  .   .  . .  ..* ..  . .     . *    ..*.

 ecolibcat,61-103  HDSAKIYRFP VSQSIDELME ACRDVIRKNN .......LTS AYIRPLIFVG
  dalanine,52-94   YASAEKIRIT IPYTKDKFHQ LLHELVEKNE .......LNT GHIYFQVTRG
humanbcatm,101-149LRSAMRLCLP .SFDKLELLE CIRRLIEVDK DWVPDAAGTS LYVRPVLIGN
                   **     .  .      .   . ..  .          .   .   .

 ecolibcat,104-153DVGMGVNPPA GYSTDVIIAA FPWGAYLGAE ALEQGIDAMV SSWNRAAPNT
  dalanine,95-143 TSPRAHQFPE NTVKPVII.G YTKENPRPLE NLEKGVKATF VEDIRWLRCD
humanbcatm,150-197EPSLGVSQPR RALLFVILC. .PVGAYFPGG SVTPVSLLAD PAFIRAWVGG
                   . .   *      **.    .    .    .          *

 ecolibcat,154-202IPTAAKAGGN YLSSLLVGSE ARRHGYQEGI ALD.VNGYIS EGAGENLFEV
  dalanine,144-186I....KSL.N LLGAVLAKQE AHEKGCYEAI .LH.RNNTVT EGSSSNVFGI
humanbcatm,198-246VGN.YKLGGN YGPTVLVQQE ALKRGCEQVL WLYGPDHQLT EVGTMNIFVY
                  .    *   *   ...*  .* * ..*  . .  *   .  .. * .. *.*

 ecolibcat,203-246...KDGV..L FTPPFTSSAL PGITRDAIIK LAKELG.IEV REQVLSRESL
  dalanine,187-230...KDGI..L YTHPANNMIL KGITRDVVIA CANEIN.MPV KEIPFTTHEA
humanbcatm,247-296WTHEDGVLEL VTPPLNGVIL PGVVRQSLLD MAQTWGEFRV VERTITMKQL
                   **.  *  * *     *  *. *. ..   *       *  *   .

 ecolibcat,247-290YLA......D EVFMSGTAAE ITPVRSVDGI QVGEGRCGPV TKRIQQAFFG
  dalanine,231-274LKM......D ELFVTSTTSE ITPVIEIDGK LIRDGKVGEW TRKLQKQFET
humanbcatm,297-343LRALEEGRVR EVFGSGTACQ VCPVHRI... LYKDRNLHIP TMENGPELIL
                          *.* ..*. . . **  .      .          *

 ecolibcat,291-308LFTGETEDKW GWLDQVNQ~~ ~~
  dalanine,275-282KIPKPLHI~~ ~~~~~~~~~~ ~~
humanbcatm,344-365RFQKELKEIQ YGIRAHEWMF PV
```

Figure 4
Sequence alignment of human BCATm, *E. coli* BCAT and D-AAT with double-underlined bold letters representing helices and single-underlined letters in italics representing β-strands. The numbering of each of the sequence is as indicated with the name.

Table 2
Root-mean-square deviations of the coordinates of the main-chain atoms of conserved secondary-structure elements between human BCAT, *E. coli* BCAT and D-AAT monomers using the program *LSQKAB* (Kabsch, 1976).

		R.m.s. deviation of main-chain atoms (Å)
Human BCAT, monomer *A*, orthorhombic form	Human BCAT, monomer *B*, orthorhombic form	0.56
Human BCAT, monomer *A*, orthorhombic form	Human BCAT, monomer *A*, monoclinic form	0.69
Human BCAT, monomer *A*, orthorhombic form	Human BCAT, monomer *A*, trigonal form	0.96
Human BCAT, monomer *A*, orthorhombic form	*E. coli* BCAT, monomer *A*	1.36 (for 20.5% of the total structure omitting side-chain atoms, termini and loops)
Human BCAT, monomer *A*, orthorhombic form	D-AAT, monomer *A*	1.78 (for 20.5% of the total structure omitting side-chain atoms, termini and loops)

The r.m.s. deviation calculated using *LSQKAB* (Kabsch, 1976) for this subset of atoms is 1.36 Å (Table 2). This demonstrates that it is possible to use the molecular-replacement method to solve very distantly related structures.

Using the refined model of the orthorhombic form, further refinement in the monoclinic form was continued. A few iterations of *CNS* refinement and model building in *O*, followed by water picking, refined the structure to an $R_{\rm cryst}$ of 16% and an $R_{\rm free}$ of 22% using 21 221 reflections to 2.5 Å resolution with a 2σ cutoff on F (Table 1). The final model comprises 2×365 residues, two PLPs and 197 water molecules.

The orthorhombic form structure also helped in completing the refinement of the trigonal form. There were 212 water molecules picked in total. Towards the final stages of the refinement the electron-density maps at the active site were most intriguing (Fig. 2). There was clearly very good density for the PLP. In addition, there was also density covalently linked to both the PLP and the active-site Lys NZ atom. The extra density arises from a Tris molecule that has covalently bridged the pyridoxal and the active-site lysine. The Tris inhibition is observed in both the monomers. The structure refined to an $R_{\rm cryst}$ of 21% and an $R_{\rm free}$ of 22% using 31 159 reflections to 2.3 Å resolution (Table 1).

Analysis of the stereochemistry of all structures with *PROCHECK* (Laskowski *et al.*, 1993) showed that 99.5% of the main-chain atoms fall within the core and generously allowed regions of the Ramachandran plot. Ser2, Ser4 and Gln316 are in the disallowed region of the Ramachandran map. There is weak density for Ser2 and Ser4 and good density for Gln316. None of these residues are close to the active site. Owing to the difference in the resolution of the data and the data-collection method, the temperature factors of the orthorhombic form are consistently higher than the monoclinic and trigonal forms. However, the temperature-factor profile as plotted *versus* residue number looks very similar.

3. Results

All the peptide bonds are *trans* except at Gly338–Pro339, where the bond is *cis* in the monoclinic and trigonal forms. The mature enzyme is a dimer, with 365 residues per subunit. Each monomer is composed of a small domain (residues 1–175) and a large domain (residues 176–365). The dimer interface comprises 37 residues from domain 1 and 19 residues from domain 2. 60% of the residues at the dimer interface are hydrophobic. On dimerization a significant percentage (28%) of the total accessible surface area is buried (4631 Å^2). The two PLP cofactors are located close to the dimer interface.

A ribbon diagram of the folding of human BCATm is shown in Fig. 3. The small domain comprises four α-helices from residues 6–10, 65–70, 92–107 and 113–132. There is a funnel-shaped twisted β-pleated sheet from residues 11–12, 37–43, 52–55, 59–61, 73–75, 78–82, 88–91, 139–148 and 161–170 of the small domain.

The large domain is built of four α-helices from residues 204–219, 268–282, 292–301 and 339–354. There is also a ten-stranded antiparallel β-pleated sheet in each of the monomers.

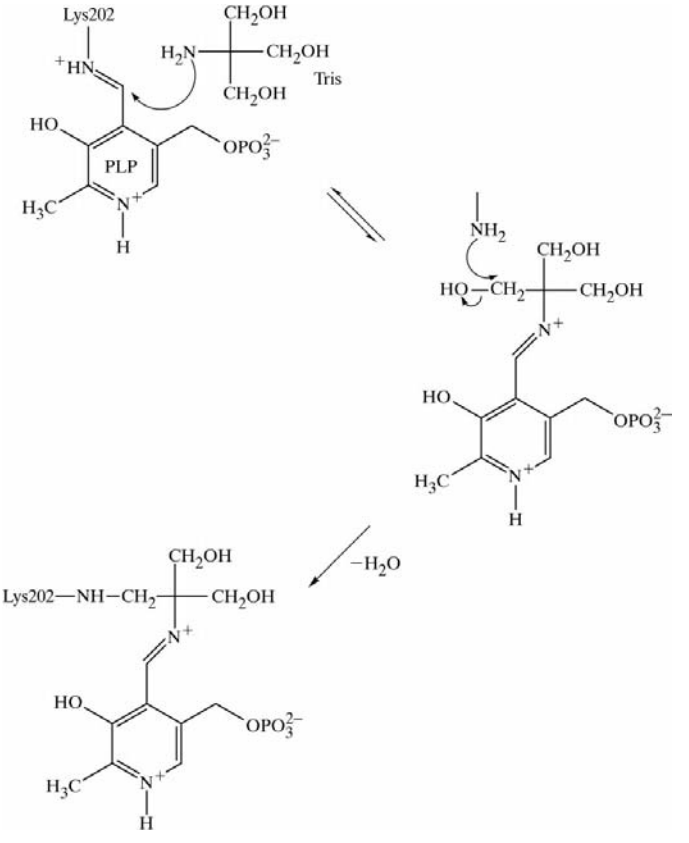

Figure 5
Hypothetical reaction mechanism between human BCATm and Tris leading to complete inactivation of the enzyme.

The strands are between residues 182–185, 224–229, 234–238, 241–248, 254–258, 285–288, 305–311, 318–324, 329–331 and 362–364.

As seen from an analysis of the contacts using the program *CONTACT* (Collaborative Computational Project, Number 4, 1994) and the symmetry-generated packing diagrams in *O* (Jones & Kjeldgaard, 1997), the dimers in the three crystal forms are packed quite differently. In the monoclinic form, the two monomers are held together by six hydrogen bonds and 12 van der Waals contacts less than 3.5 Å (compared with ten and 13, respectively, in the orthorhombic form and eight and 12, respectively, in the trigonal form). All of these interactions involve side-chain atoms. In all three forms, the residues involved in hydrogen bonding and aiding in holding the dimer together are His69, Tyr70, Ser71, Gln73 and Arg143. As discussed below, interaction between Tyr70 from the second monomer and Arg143 of the first monomer seem crucial for the formation of the putative substrate-binding pocket (Fig. 8*a*) and provide a structural explanation for the activity of the enzyme as a dimer. There are additional hydrogen bonds between the monomers in the orthorhombic and the trigonal forms involving the side chains of Gln157, Trp194 and Gln215.

Fig. 4 shows the alignment of human BCATm, *E. coli* BCAT and D-AAT with secondary-structure elements marked for each of the proteins. The overall folding topology of human BCATm is very similar to that of *E. coli* BCAT and D-AAT. However, on close inspection one can see changes in secondary-structure elements. Of the six fairly long helices, five have increased in length in human BCATm compared with *E. coli* BCAT. Most obvious are the helices starting at residues 113 and 292. There are 33 more residues at the N-terminus, lengthening the β-sheet strands and extending them by two more strands. Most of the loops have increased lengths and altered conformations. The electron density for the loop connecting the small domain and the large domain (residues 172–179) is weak for monomer *A* but fairly good for monomer *B* in both of the PLP forms. In the Tris-inhibited structure the loops have much better density. This loop was completely disordered in the PLP form of the *E. coli* BCAT structure (Okada *et al.*, 1997).

None of the short helical stretches in human BCAT have counterparts in the *E. coli* BCAT structure and *vice versa*. Also, the long helices have C^{α} atoms deviating by as much as 5 Å from the equivalent atoms in the *E. coli* BCAT structure. The variability in the length of the helices is also reflected in the length of the strands. Short strands have disappeared in one or other of the structures. Most of the β-strands are longer in human BCATm compared with their counterparts in *E. coli* BCAT and D-AAT. The small domain in the *E. coli* BCAT has two strands less compared with the small domain in human BCATm and the large domain has three strands less than the human BCATm structure. The β-sheet regions superpose better at regions away from the N-terminus, wherein they lengthen quite a bit to incorporate the extra residues in the human BCATm sequence.

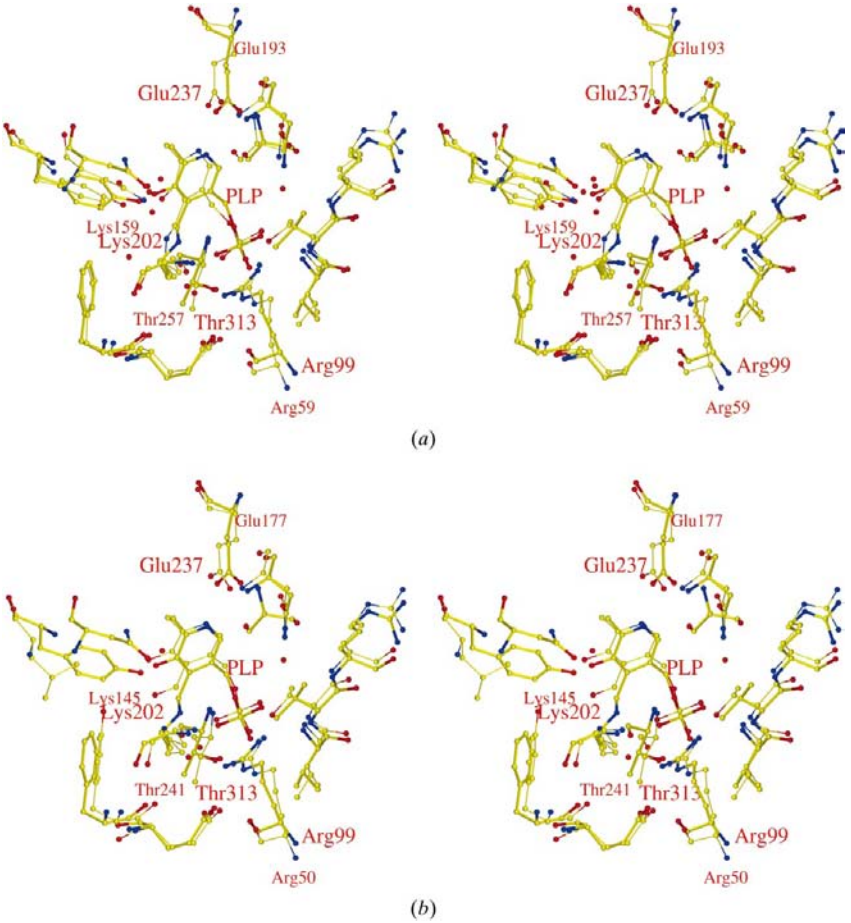

Figure 6
(*a*) Active-site superposition of *E. coli* BCAT (thinner bonds and smaller residue labels) with human BCATm (thicker bonds and larger residue labels). The side chains are conserved and their orientation is very similar. (*b*) Active-site superposition of D-AAT (thinner bonds and smaller residue labels) with human BCATm (thicker bonds and larger residue labels). Only the side chains interacting with the PLP are similar in nature and have comparable conformation.

3.1. The active site

The coenzyme, PLP, resides at the domain interface and at the bottom of the active-site pocket. Lys202 lies on the *Re* face of the coenzyme, acting as the base to abstract the α-proton. In the yellow crystals, the 4′-aldehyde of the PLP cofactor is covalently linked to the ε-amino group of the active-site lysine *via* a Schiff-base linkage (Fig. 1). Hydrogen bonds with the side chains of

Glu237 and Tyr207 anchor the PLP ring tightly at the bottom of the active-site cavity. Each of the terminal O atoms on the phosphates are held in place by two to three hydrogen bonds. The residues interacting with the phosphate O atoms are Thr313, Arg99, Val269 and Val270. In addition, there are two water molecules WAT1 and WAT21 (monomer *A* of orthorhombic structure) hydrogen bonding.

In the colorless crystals, an unbiased electron-density picture of the active site (Fig. 2) shows the convincing density for the Tris inhibitor. Both the monomers are inhibited by Tris in a similar fashion. The PLP ring is rotated by 18.6° and the centroid of the ring moves by 0.3 Å compared with the PLP structure to make room for the Tris atoms. This kind of ring rotation is also seen in the structures of D-AAT (Peisach *et al.*, 1998) and AspAT (Rhee *et al.*, 1997) with substrates. This movement of the ring leads to changes in the conformation of the two residues interacting directly with the ring, Glu237 and Tyr207. While the plane of the carboxylate of the Glu237 side chain rotates by almost 59.0° in the inhibited active site, the bulkier ring of Tyr207 rotates subtly by 8.1°. Arg192, which is interacting with Glu237 in the native structure, also rotates somewhat so as to still be able to hydrogen bond with the Glu237 side chain. The phosphates, as expected, have not moved in the two structures. At the Tris, there is rotation of

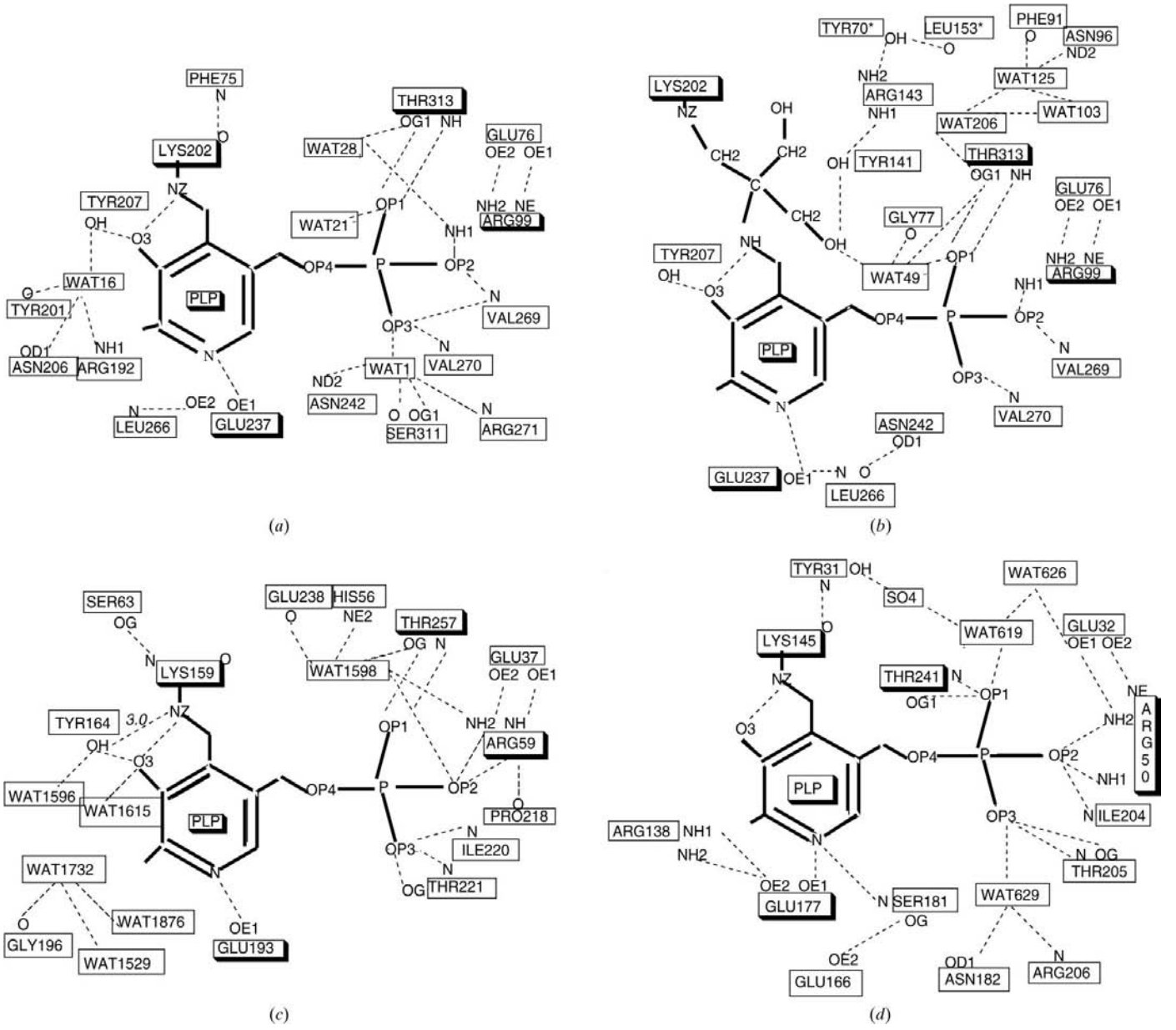

Figure 7
Schematic diagram showing the active-site interactions in (*a*) human BCATm, (*b*) Tris-inhibited human BCATm, (*c*) *E. coli* BCAT and (*d*) D-AAT. Atom names are given by PDB convention. Hydrogen-bonding distances are given for interactions less than 3.4 Å. Highlighted boxes represent residues with similar interactions in all the three enzymes.

the guanidinium moiety of the Arg43 side chain, with the hydrogen-bond network of waters changing a little compared with the native structure. One of the Tris hydroxyl groups is stabilized by hydrogen bonding with water on one end and Tyr141 on the other end. The water molecule is, in turn, hydrogen bonded to one of the O atoms of the phosphate (OP1).

The probable reaction mechanism leading to the Tris intermediate is shown in Fig. 5. It appears to be a two-step process, with the removal of a water molecule at the second step leading to the inactive intermediate. The fact that a small molecule like Tris has reacted in an unexpected fashion is not surprising. There are 13 other structures in the PDB wherein Tris has been seen to bind to the protein, three out of which comment that it was inhibiting the active site (PDB codes 1ayx, 1cpf and 1arm). However, this is the first example wherein Tris is covalently linked to the active-site residue and irreversibly inhibits the enzyme.

As seen in the superposition diagrams of the active sites of human BCATm, *E. coli* BCAT and D-AAT (Fig. 6), most of the active-site residues at the PLP end of the active site are either conserved or similar. Although the side-chain disposition is comparable, there are changes at the active site induced by the waters which alter the hydrogen-bonding interactions (Fig. 7). These changes could be significant enough to alter reaction rates and binding constants with substrates. The PLP is deeply buried within the protein matrix and is involved in many specific interactions which have counterparts in all other PLP enzymes which share this fold. Three of these interactions are conserved between human BCATm, *E. coli* BCAT and D-AAT, anchoring the pyridine ring and the phosphates such that proton transfer occurs on the *Re* face of PLP. They are the interactions involving Glu237, Arg99 and Thr313 highlighted in Fig. 7. While residues from the second monomer approaching the active site of the first monomer may be important for substrate binding, they do not have any direct interactions with the PLP itself. Interestingly, most of the residues at the active site interacting with the coenzyme are from the large domain.

Differences in the three fold-type IV proteins are seen in the interactions of the O3 atom of the PLP (Fig. 7). In the human BCATm, it is hydrogen bonded to the hydroxyl group of Tyr207 and Lys202 NZ (Fig. 7*a*). In the *E. coli* BCAT active site, the conserved residues Tyr164 and Lys159 take analogous places (Fig. 7*c*). In addition, the O3 atom also hydrogen bonds to a water molecule, WAT1615. In the case of D-AAT, the O3 atom hydrogen bonds to Lys145 NZ only (Fig. 7*d*).

As shown in Figs. 7(*a*), 7(*c*) and 7(*d*), each of the phosphate O atoms in all the three structures form two to three hydrogen bonds. Therefore, it is no surprise that it might be quite difficult to dislodge the PLP from the active site in solution. The phosphate O atoms OP1 and OP3 have bound waters in the D-AAT and human BCATm structures. In the *E. coli* BCAT the other phosphate O atom OP2 has a hydrogen-bonded water which is not found with OP1 or OP3. Although not conserved, most of the residues interacting with the phosphates are very similar (see Fig. 7).

The pyridine ring of the PLP is sandwiched between Leu266 (Leu217 in *E. coli* BCAT and Leu201 in D-AAT) on one face and the peptide plane of Thr240–Met241 (Gly196–Glu197 in *E. coli*, Ser180–Ser181 in D-AAT) on the other. The recent structure of the L201A mutant of D-AAT (Sugio *et al.*, 1998) has shown that D-AAT Leu201 plays a crucial role in the transamination reaction by keeping the pyridoxal ring in the proper location.

Sequence-alignment comparison between mitochondrial and cytosolic human BCAT isoenzymes shows that, except for Tyr201 (replaced by Cys) and Val270 (replaced by Thr), the other residues interacting with the PLP in the active site are identical. As seen in the active-site cartoons (Fig. 7), it is the backbone of residues Val270 and Tyr201 that are interacting and not the side chains. Hence, even these changes in the BCATc sequence might not disrupt the hydrogen-bonding pattern of the active site in a significant way. The active site of human cytosolic BCAT at the PLP end will probably look very much like the active site in the mitochondrial enzyme. On the other hand, the specificity of gabapentin for the BCATc isoenzyme suggests there must be differences in the substrate-binding pockets in the two proteins.

Comparison of the substrate-binding pocket in D-AAT and the putative substrate-binding pocket in human BCATm shows that the D-amino acids probably approach the active site in a direction opposite to the L-amino acids (Peisach *et al.*, 1998). Fig. 8 shows the putative substrate-binding pocket with the proteins superposed to the best least-squares fit using the program *LSQKAB* (Kabsch, 1976).

The substrate-binding pocket could be imagined to have two halves as seen in the substrate-bound structure of D-AAT (Fig. 8*b*). One half of the surface is lined predominantly by more hydrogen-bonding side chains (His100 from monomer *B*, Arg98 from monomer *B* and Tyr31) than the other (Val33, Thr242 and Ser240). The α-carboxylate group interacts with the former surface in D-AAT. In the human BCATm this surface of the putative substrate-binding pocket is lined by predominantly hydrophobic side chains Phe75, Tyr207 and Tyr70 (from the second monomer), making it a favourable anchor for the branched-chain amino-acid side chains. This would mean that the L-amino acids and D-amino acids approach the active site in opposite directions. As seen in Fig. 8(*a*), Thr313, Tyr141 and Arg143 are the likely residues that might stabilize the α-carboxylate group of the substrate. Tyr70 from monomer *B* hydrogen bonds with Arg143 from monomer *A* to complete the formation of the surface of the substrate-binding pocket.

4. Conclusions

The new crystal structures of human mitochondrial BCATm reported here show that it folds in a fashion similar to *E. coli* BCAT and D-AAT. The active site of the three PLP-dependent enzymes also shows comparable hydrogen-bonding interactions with their cofactors, except for changes owing to waters. The residues lining the putative substrate-binding

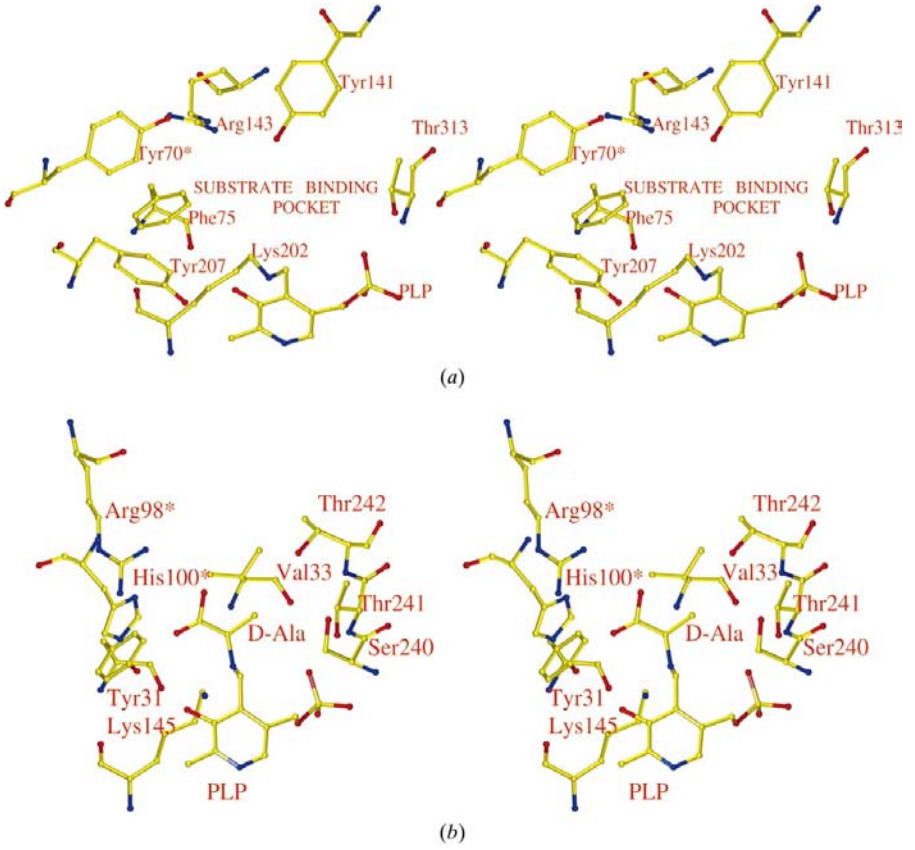

Figure 8
(*a*) Putative substrate-binding pocket in human BCATm and (*b*) D-Ala bound to D-AAT in the crystal structure PDB code 3daa. The PLP and the rest of the protein have been superposed to the best least-squares fit using the program *LSQKAB* (Kabsch, 1976) from the *CCP*4 program suite (Collaborative Computational Project, Number 4, 1994). In the human enzyme the crucial hydrogen bond between Arg143 and Tyr70 from the second monomer helps in forming the substrate pocket. The L-amino acids and D-amino acids probably approach the active site in opposite directions, as the residues lining the pocket are complementary in nature (Peisach *et al.*, 1998).

pocket show complementary properties, suggesting that the L- and D-amino acids approach the active site in opposite directions.

We wish to thank NIH (grant DK34738) and Parke Davis pharmaceuticals for the funding of this project. Use of the Advanced Photon Source was supported by the US Department of Energy, Basic Energy Sciences, Office of Energy Research under contract number W-31-109-ENG-38. Thanks also to Dr Andrew Howard at the APS, Dr Penny Drown at Wake Forest University School of Medicine and Dr Hemant Yennawar at Penn State University for giving of their time and expertise at various stages of the project. Special thanks to Dr Ken Hirotsu for providing the coordinates of the *E. coli* BCAT prior to their release.

References

Bledsoe, R. K., Dawson, P. A. & Hutson, S. M. (1997). *Biochim. Biophys. Acta*, **1339**, 9–13.
Brünger, A. T. (1992). *X-PLOR Version* 3.1. *A System for X-ray Crystallography and NMR*. New Haven, CT, USA: Yale University Press.
Brunger, A. T., Adams, P. D., Clore, G. M., DeLano, W. L., Gros, P., Grosse-Kunstleve, R. W., Jiang, J. S., Kuszewski, J., Nilges, M., Pannu, N. S., Read, R. J., Rice, L. M., Simonson, T. & Warren, G. L. (1998). *Acta Cryst.* D**54**, 905–921.
Collaborative Computational Project, Number 4 (1994). *Acta Cryst.* D**50**, 760–763.
Cowtan, K. D. & Main, P. (1996). *Acta Cryst.* D**52**, 43–48.
Davoodi, G. D., Drown, P. M., Bledsoe, R. K., Wallin, R., Reinhart, G. D. & Hutson, S. M. (1998). *J. Biol. Chem.* **273**, 4982–4989.
Faure, M., Glomot, F., Bledsoe, R., Hutson, S. M. & Papet, I. (1999). *Eur. J. Biochem.* **259**, 104–111.
Grishin, N. V., Phillips, M. A. & Goldsmith, E. J. (1995). *Protein Sci.* **4**, 1291–1304.
Hall, T. R., Wallin, R., Reinhart, G. D. & Hutson, S. M. (1993). *J. Biol. Chem.* **268**, 3092–3098.
Harper, A. E. (1989). *Ann. NY Acad. Sci.* **573**, 267–273.
Howlin, B., Butler, S. A., Moss, D. S., Harris, G. W. & Driessen, H. P. C. (1993). *J. Appl. Cryst.* **26**, 622–624.
Hutson, S. M., Berkich, D., Drown, P., Xu, B., Aschner, M. & LaNoue, F. (1998). *J. Neurochem.* **71**, 863–874.
Hutson, S. M., Bledsoe, R. K., Hall, T. R. & Dawson, P. A. (1995). *J. Biol. Chem.* **270**, 30344–30352.
Hutson, S. M., Fenstermacher, D. & Mahar, C. (1988). *J. Biol. Chem.* **263**, 3618–3625.
Ichihara, A. (1985). *Aminotransferases of Branched Chain Amino Acids in Transaminases*, Vol. 2, edited by P. Christen & D. E. Metzler, pp. 430–439. New York: John Wiley & Sons.
Jager, J., Moser, M., Sauder, U. & Jansonius, J. N. (1994). *J. Mol. Biol.* **239**, 285–305.
Jones, T. A. & Kjeldgaard, M. (1997). *Methods Enzymol.* **277**, 173–208.
Kabsch, W. (1976). *Acta Cryst.* A**32**, 922–923.
Kleywegt, G. J. & Jones, T. A. (1997). *Methods Enzymol.* **277**, 208–230.
Laskowski, R. A., MacArthur, M. W., Moss, D. S. & Thornton, J. M. (1993). *J. Appl. Cryst.* **26**, 283–291.
McPhalen, C. A., Vincent, M. G. & Jansonius, J. N. (1992). *J. Mol. Biol.* **225**, 495–517.
Malashkevich, V. N., Strokopytov, B. V., Borisov, V. V., Dauter, Z., Wilson, K. S. & Torchinsky, Y. M. (1995). *J. Mol. Biol.* **247**, 111–124.
Malashkevich, V. N., Toney, M. D. & Jansonius, J. N. (1993). *Biochemistry*, **32**, 13451–13462.
Miyahara, I., Hirotsu, K., Hayashi, H. & Kagamiyama, H. (1994). *J. Biochem.* **116**, 1001–1012.
Nakai, T., Mizutani, H., Miyahara, I., Hirotsu, K., Takeda, S., Jhee, K.-H., Yoshimura, T. & Esaki, N. (2000). *J. Biochem.* **128**, 29–38.
Navaza, J. (1994). *Acta Cryst.* A**50**, 157–163.
Okada, K., Hirotsu, K., Sato, M., Hayashi, H. & Kagamiyama, H. (1997). *J. Biochem.* **121**, 637–641.

Okamoto, A., Higuchi, T., Hirotsu, K., Kuramitsu, S. & Kagamiyama, H. (1994). *J. Biochem.* **116**, 95–107.
Otwinowski, Z. & Minor, W. (1996). *Method Enzymol.* **276**, 307–326.
Peisach, D., Chipman, D. M., Van Ophem, P. W., Manning, J. M. & Ringe, D. (1998). *Biochemistry*, **37**, 4958–4967.
Rhee, S., Silva, M. M., Hyde, C. C., Rogers, P. H., Metzler, C. M., Metzler, D. E. & Arnone, A. (1997). *J. Biol. Chem.* **272**, 17293–17302.
Schuldiner, O., Eden, A., Ben-Yosef, T., Yanuka, O., Simchen, G. & Benvenisty, N. (1996). *Proc. Natl Acad. Sci. USA*, **93**, 7143–7148.
Sugio, S., Kashima, A., Kishimoto, K., Peisach, D., Petsko, G. A., Ringe, D., Yoshimura, T. & Esaki, N. (1998). *Protein Eng.* **11**, 613–619.
Sugio, S., Petsko, G. A., Manning, J. M., Soda, K. & Ringe, D. (1995). *Biochemistry*, **34**, 9661–9669.
Wallin, R., Hall, T. R. & Hutson, S. M. (1990). *J. Biol. Chem.* **265**, 6019–6024.
Welty, D. F., Schielke, G. P. & Rothstein, J. D. (1995). *Ann. Pharmacother.* **29** 1164–1167.
Yoshimura, T., Nishimura, K., Ito, J., Esaki, N., Kagamiyama, H., Manning, J. M. & Soda, K. (1993). *J. Am. Chem. Soc.* **115**, 3897–390.